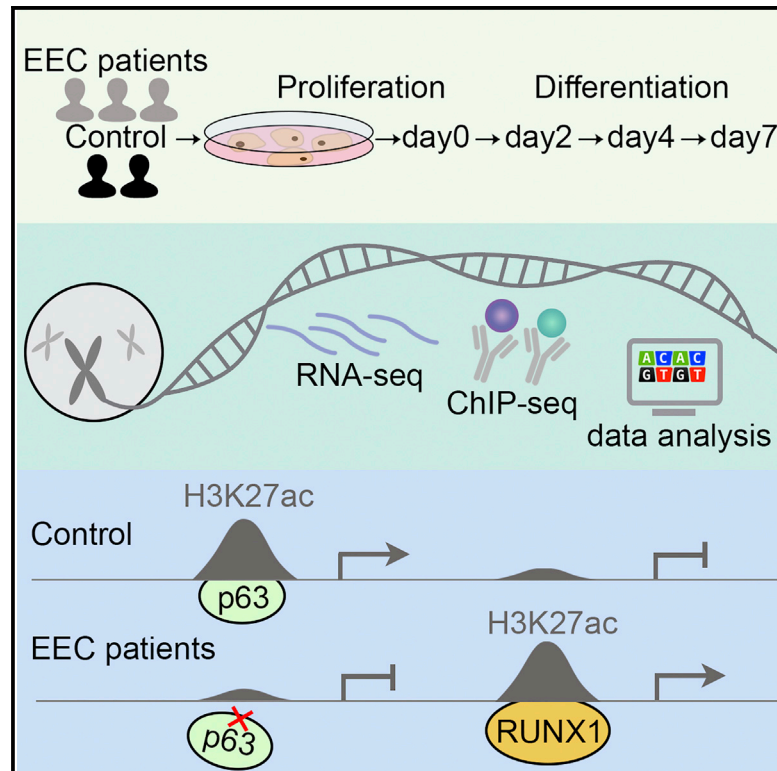


## Mutant p63 Affects Epidermal Cell Identity through Rewiring the Enhancer Landscape

### Graphical Abstract



### Authors

Jieqiong Qu, Sabine E.J. Tanis, Jos P.H. Smits, ..., Hans van Bokhoven, Klaas W. Mulder, Huiqing Zhou

### Correspondence

jo.zhou@radboudumc.nl

### In Brief

Using transcriptomics and epigenomics, Qu et al. elucidate how mutant p63 associated with EEC syndrome alters the enhancer landscape in skin keratinocytes. The genome-wide redistribution of enhancers leads to the downregulation of epidermal genes and upregulation of non-epidermal genes and affects the cell identity of skin keratinocytes.

### Highlights

- Downregulated epidermal genes and upregulated non-epidermal genes in EEC keratinocytes
- A genome-wide redistribution of enhancers in EEC keratinocytes
- Gained enhancers are frequently bound by deregulated RUNX1 in EEC keratinocytes
- siRUNX1 partially rescues gene deregulation and the altered enhancer landscape



# Mutant p63 Affects Epidermal Cell Identity through Rewiring the Enhancer Landscape

Jieqiong Qu,<sup>1</sup> Sabine E.J. Tanis,<sup>1,6</sup> Jos P.H. Smits,<sup>2,6</sup> Evelyn N. Kouwenhoven,<sup>1</sup> Martin Oti,<sup>1</sup> Ellen H. van den Bogaard,<sup>2</sup> Colin Logie,<sup>3</sup> Hendrik G. Stunnenberg,<sup>3</sup> Hans van Bokhoven,<sup>4,5</sup> Klaas W. Mulder,<sup>1</sup> and Huiqing Zhou<sup>1,4,7,\*</sup>

<sup>1</sup>Department of Molecular Developmental Biology, Faculty of Science, Radboud Institute for Molecular Life Sciences, Radboud University, Nijmegen, the Netherlands

<sup>2</sup>Department of Dermatology, Radboud Institute for Molecular Life Sciences, Radboud University Medical Center, Nijmegen, the Netherlands

<sup>3</sup>Department of Molecular Biology, Faculty of Science, Radboud Institute for Molecular Life Sciences, Radboud University, Nijmegen, the Netherlands

<sup>4</sup>Department of Human Genetics, Radboud University Medical Center, Nijmegen, the Netherlands

<sup>5</sup>Department of Cognitive Neurosciences, Donders Institute for Brain, Cognition and Behaviour, Radboud University Medical Center, Nijmegen, the Netherlands

<sup>6</sup>These authors contributed equally

<sup>7</sup>Lead Contact

\*Correspondence: [jo.zhou@radboudumc.nl](mailto:jo.zhou@radboudumc.nl)  
<https://doi.org/10.1016/j.celrep.2018.11.039>

## SUMMARY

Transcription factor p63 is a key regulator of epidermal keratinocyte proliferation and differentiation. Mutations in the p63 DNA-binding domain are associated with ectrodactyly, ectodermal dysplasia, and cleft lip/palate (EEC) syndrome. However, the underlying molecular mechanism of these mutations remains unclear. Here, we characterized the transcriptome and epigenome of p63 mutant keratinocytes derived from EEC patients. The transcriptome of p63 mutant keratinocytes deviated from the normal epidermal cell identity. Epigenomic analyses showed an altered enhancer landscape in p63 mutant keratinocytes contributed by loss of p63-bound active enhancers and unexpected gain of enhancers. The gained enhancers were frequently bound by deregulated transcription factors such as RUNX1. Reversing RUNX1 overexpression partially rescued deregulated gene expression and the altered enhancer landscape. Our findings identify a disease mechanism whereby mutant p63 rewires the enhancer landscape and affects epidermal cell identity, consolidating the pivotal role of p63 in controlling the enhancer landscape of epidermal keratinocytes.

## INTRODUCTION

The transcription factor (TF) p63 is an ancient member of the p53 gene family. Different from p53 that has a convincing function in tumor suppression, p63 is a key regulator of development of the epidermis, specifically in epidermal stem cell self-renewal, morphogenesis, and directing differentiation programs (Candi et al., 2008; Mills et al., 1999; Yang et al., 1999). Several p63 iso-

forms have been reported, and all isoforms contain the DNA-binding domain (Kouwenhoven et al., 2015b).

The role of p63 in epidermal development has been established by two independent p63 knockout mouse models (Mills et al., 1999; Yang et al., 1999). These p63-deficient mice do not have the epidermis and epidermal-related appendages. During embryonic development, p63-deficient mice develop a normal ectoderm with Krt8- and Krt18-positive simple epithelial cells. However, they fail to initiate embryonic stratification or produce mature Krt5- and Krt14-positive epithelial and epidermal cells, termed keratinocytes (Shalom-Feuerstein et al., 2011). These findings demonstrate that p63 is essential and required for the commitment to a proper epidermal cell fate during development.

In keratinocytes, p63 plays important roles in both proliferation and differentiation. The p63 protein, mainly the  $\Delta Np63\alpha$  isoform, is expressed at a high level in proliferating keratinocytes in the basal layer of the epidermis. Upon stratification, its expression level is reduced (Candi et al., 2007). Knockdown of p63 in keratinocytes affects proliferation and prevents cells from differentiation (Truong et al., 2006). At the molecular level, knockdown of p63 induces genes controlling cell-cycle arrest, such as p21 (CDKN1A) (LeBoeuf et al., 2010), and downregulates genes that are important for epidermal differentiation, such as *PERP* and *KRT14* (Ihrle et al., 2005; Romano et al., 2007). These data show that p63 represses cell-cycle-arrest genes to promote proliferation and activates epidermal differentiation genes to induce differentiation.

In recent years, a number of epigenomic profiling studies established the master regulator role of p63 in the genome of keratinocytes, predominantly in controlling enhancers (Bao et al., 2015; Kouwenhoven et al., 2015a; Rinaldi et al., 2016). p63 bookmarks genomic loci and cooperates with specific TFs to activate epidermal genes via active enhancers. Consistently, transposase accessible chromatin with high-throughput sequencing (ATAC-seq) analysis showed that p63-binding sites are preferentially located in nucleosome-enriched regions in epidermal keratinocytes, and these sites are inaccessible in cell types where



p63 is not expressed (Bao et al., 2015). In keratinocytes, p63 cooperates with an ATP-dependent chromatin remodeling factor, BAF1, to make these regions accessible. It has also been shown that p63 directly regulates chromatin factors such as Satb1 and Brg1 that play roles in higher-order chromatin remodeling, covalent histone modifications, and nuclear assembly (Fessing et al., 2011; Mardaryev et al., 2014). These data suggest that p63 regulates epidermal cell fate determination and differentiation not only through direct target genes but also via modulating the chromatin landscape.

The key role of p63 in epidermal development has also been demonstrated in human disease models. Heterozygous mutations of *TP63* encoding p63 cause a spectrum of developmental disorders. Among them, ectrodactyly, ectodermal dysplasia, and cleft lip/palate (EEC) syndrome is caused by point mutations located in the p63 DNA-binding domain and manifests ectodermal dysplasia with defects in the epidermis and epidermal-related appendages, limb malformation, and cleft lip and/or palate (Rinne et al., 2007). Five hotspot mutations affecting amino acids, R204, R227, R279, R280, and R304, have been found in ~90% of the EEC population, and these EEC mutations were shown to disrupt p63 DNA binding and result in impaired transactivation activity (Browne et al., 2011; Celli et al., 1999). Therefore, these mutant p63 proteins have been proposed to have a dominant-negative effect on wild-type p63, probably by abolishing DNA binding as a result of tetramerization of wild-type and mutant proteins (Brunner et al., 2002). Furthermore, mouse genetic studies support the dominant-negative model. Heterozygous p63 knockout mice do not show any ectodermal phenotype (Mills et al., 1999; Yang et al., 1999), whereas heterozygous knockin mice carrying an EEC mutation resemble the human phenotype (Vernersson Lindahl et al., 2013).

Although the role of p63 in normal epidermal development and differentiation has been demonstrated, the molecular mechanism by which p63 mutations cause the epidermal phenotype in diseases is not yet understood. We previously reported that p63 mutant keratinocytes derived from EEC patients could not fully differentiate toward terminal stratification in both 2D and 3D cellular models (Shen et al., 2013). In this study, EEC patient keratinocytes carrying three hotspot mutations (R204W, R279H, and R304W) were assessed by transcriptomic and epigenomic analyses to identify the underlying molecular mechanism. Our data showed that deregulated gene expression accompanied by a rewired enhancer landscape leads to a less defined epidermal cell identity of p63 mutant keratinocytes, which potentially contributes to the pathogenic mechanism of EEC syndrome.

## RESULTS

### Loss of Characteristic Epidermal Expression Profiles in p63 Mutant Keratinocytes

Using an established *in vitro* differentiation model of epidermal keratinocytes (Kouwenhoven et al., 2015a), we characterized gene expression differences between keratinocytes derived from non-EEC individuals (control) and EEC patients carrying mutations in the DNA-binding domain of p63 (R204W, R279H, and R304W, p63 mutant) (Figures 1A and 1B). Similar to our pre-

vious report (Shen et al., 2013), p63 mutant keratinocytes retained largely unchanged morphology at the terminal stage of differentiation compared to the multilayer cell structures of control keratinocytes on day 7 (Figure S1A), indicating that they were unable to fully differentiate. To better characterize these mutant keratinocytes at the molecular level, we performed RNA-sequencing (RNA-seq) analyses. In principal-component analysis (PCA), gene expression of control keratinocytes from day 0 to day 7 moved along the principle component 1 (PC1) axis (51%) that probably defines the differentiation process, whereas mutant keratinocytes remained at the left side of PC1 (Figure 1C). Consistently, DAVID Gene Ontology (GO) annotation (Dennis et al., 2003) of the top 500 genes associated with PC1 showed terms related to epidermis development and keratinocyte differentiation (Tables S1A and S1B). Many deregulated genes were validated by qRT-PCR and at the protein level (Figure S1B). These molecular data confirmed the differentiation defect of p63 mutant keratinocytes.

We next analyzed differentially expressed (DE) genes ( $p < 0.05$ ) between control and p63 mutant keratinocytes during differentiation. Overall, 3,373 genes were upregulated and 4,595 genes were downregulated in p63 mutant keratinocytes (Table S1D), which were distinguished into four clusters (Figure 1D; Table S1E). Among the upregulated genes (EC1), some were generally not expressed or expressed at a low level in control keratinocytes. There was an enrichment of genes involved in extracellular structure organization, actin cytoskeleton organization, and muscle cell function (e.g., *ACTG1* and *MYH10*) (Table S1F). TF genes in this cluster include *SOX4*, *TEAD2*, and *RUNX1*, which are widely expressed in many cell types, and a number of Antp homeobox family members, such as *HOX* genes. Interestingly, *TP63* was also detected in EC1, and  $\Delta$ Np63 was the isoform detected in both control and mutant keratinocytes (Figure S1C). Compared to the decreased p63 expression during differentiation in control keratinocytes, an increased p63 expression at the proliferation stage was observed in p63 mutant keratinocytes, and this expression level stayed at a high level through differentiation (Figure S1C).

The 4,595 downregulated genes whose expression was dynamically induced during differentiation in control keratinocytes remained low and largely unchanged in p63 mutant keratinocytes. These genes were grouped into three clusters (EC2, EC3, and EC4) (Tables S1G–S1I). Genes in EC2 showed a sharp increase in gene expression on day 7 in control keratinocytes. Many of these genes were involved in catabolic pathways and cell death (e.g., *UBE4A* and *CDKN2D*). Genes in EC3 were highly expressed at the proliferation stage on day 0, and expression went down during differentiation. They were mainly involved in cell-cycle regulation (e.g., *CDC20* and *KIFC1*). Finally, genes in EC4 showed a progressive upregulation in control keratinocytes, and many of them were involved in ectoderm development and keratinocyte differentiation. The TF genes in this cluster included *OVOL1* and *KLF4*, and known p63 co-regulators, such as *TFAP2A* and *NFE2L2*. Of note, consistent with the morphological changes (Figure S1A), the deregulated gene expression was more evident in mutant keratinocytes carrying R204W and R304W than those carrying R279H (Figure 1D). Taken together, our RNA-seq analyses showed downregulation of epidermal

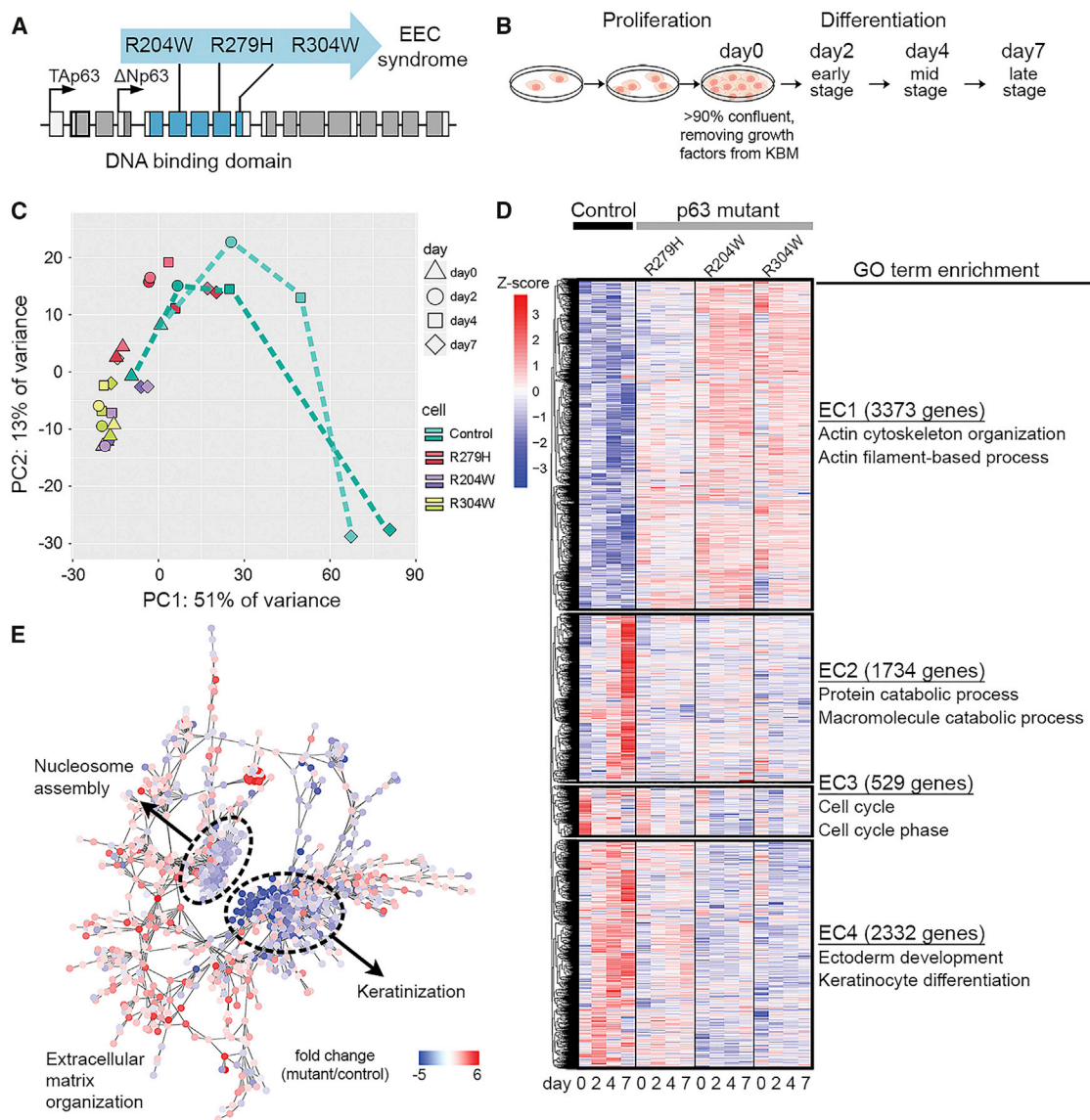


**Figure 1. Transcriptome Dynamics of Control and p63 Mutant Keratinocytes during Differentiation**

(A) EEC p63 mutant keratinocytes used in this study.

(B) The setup of *in vitro* differentiation of epidermal keratinocytes.

(C) Principal-component analysis (PCA) on RNA-seq data. Two independent control lines and three p63 mutant lines are indicated with different colors. Shapes indicate four stages.

(D) Hierarchical clustering of differentially expressed genes ( $p < 0.05$ ). The Z score was calculated based on  $\log_{10}$  (fragments per kilobase per million reads mapped [FPKM] + 0.01) of each gene. Enriched top two Gene Ontology (GO) terms of genes per gene expression cluster (EC) are shown.

(E) Coexpression network of deregulated genes in p63 mutant keratinocytes during differentiation. Interactions with connectivity weight  $> 0.1$  were shown. Two main co-expression modules were labeled with corresponding GO terms. The node color indicates the expression fold change between mutant and control keratinocytes.

See also [Figures S1](#) and [S2](#) and [Table S1](#).

differentiation genes and upregulation of non-epidermal genes in p63 mutant keratinocytes, suggesting that p63 mutant keratinocytes have a less defined epidermal cell identity.

To better visualize the interaction between DE genes, we carried out weighted gene-coexpression correlation network analyses using the Cytoscape Network Analyzer ([Tables S1J](#) and [S1K](#)). Two significant coexpression modules were identified, of

which many genes were involved in keratinization (e.g., *LOR* and *FLG*) and nucleosome assembly ([Figures 1E](#) and [S2A](#); [Table S1L](#)). Most genes in both modules showed downregulated expression in p63 mutant keratinocytes. The upregulated genes in p63 mutant keratinocytes did not generate significant main modules but generated several small subnetwork modules. They likely played roles in extracellular matrix organization

(Table S1L). However, the higher inter-modular connectivity between keratinization, nucleosome assembly, and extracellular matrix organization modules suggests a biological relationship between these modules, indicating that changes in the chromatin landscape may contribute to gene deregulation. Consistent with this notion, many chromatin regulators were deregulated in p63 mutant keratinocytes (Figure S2B). These factors include *KAT2B*, which is a histone acetyltransferase, and *SMYD3*, which encodes a histone methyltransferase. The deregulation of these genes was confirmed with qRT-PCR (Figure S2C).

### p63 Orchestrates Enhancer Dynamics during Epidermal Differentiation

Given the indicated relationship between p63 and the chromatin landscape, we first assessed the role of p63 in regulating the chromatin landscape during normal epidermal differentiation. We mapped histone modifications H3K27ac, H3K4me3, and H3K27me3, as well as p63 binding sites (BSs) of control keratinocytes, to open chromatin regions detected by DNase I hypersensitivity sites (DHSs) in normal human epidermal keratinocytes (NHEK) reported by ENCODE (Table S2). Two clusters of active enhancers (C3 and C4) were bound by p63 (Figures S3A–S3C). Regions in C3 showed higher p63-binding signals. GO annotation using the Genomic Regions Enrichment of Annotation Tool (GREAT), which permits functional interpretation of *cis*-regulatory regions (McLean et al., 2010), showed that nearby genes were involved in apoptosis and epidermis development. Regions in C4 had relatively lower p63-binding signals, and nearby genes were involved in keratinocyte differentiation (Figure S3C). Furthermore, cluster C7 represents a small group of open chromatin regions with H3K27me3 signals but devoid of p63 binding (Figure S3A). Genes near these regions were associated with “pattern specification process,” such as neuron fate commitment (Figure S3C).

To quantify chromatin dynamics, we used ChromHMM (Ernst and Kellis, 2012) to analyze chromatin state transitions. With the combination of H3K27ac, H3K4me3, and H3K27me3, we obtained six classes of chromatin state: active enhancers, active promoters, weak promoters, heterochromatin regions, bivalent promoters, and “unmodified” regions that were not decorated with any of the three modifications (Figure 2A; Tables S2B and S2C). By pairwise comparison between two adjacent stages of differentiation, we observed major transitions between active enhancers and unmodified regions as well as between unmodified regions and heterochromatin regions (Figure 2B). As expected, we found that the transition from unmodified regions to active enhancers was generally associated with gene upregulation; vice versa, the transition from active enhancers to unmodified regions was associated with gene downregulation, at least at early differentiation stages (days 0–2 and days 2–4) (Figure 2C), such as regulation of *LOR* (Figure 2D) and *KRT1* (Figure S3D). Furthermore, there were also transitions between active promoters and unmodified regions (Figure S3E). Interestingly, many genes that are known to be expressed in cells of mesodermal origin (e.g., *PAX2*) were heavily marked by H3K27me3 in proliferating keratinocytes (day 0). The repression was relieved at the end of the terminal differentiation of keratinocytes (Figure S3F).

Next, we asked whether specific TFs control enhancer dynamics during differentiation. Therefore, we performed motif analysis of dynamic enhancers using the HOMER package (Figure 2E). We observed that bZIP, p53 or p63, Zinc finger (Zf), and TEA motifs were enriched in regions being activated from unmodified regions on day 0 to active enhancers on day 2, while p53 or p63 was the only enriched motif in regions being activated from unmodified regions on day 2 to active enhancers on day 4. The bZIP motif was predominantly enriched in regions being activated from unmodified regions on day 4 to active enhancers on day 7, whereas the p53 or p63 motif was the only enriched motif in regions changing from active enhancers on day 4 to unmodified regions on day 7 (Figure 2E). The temporal enrichment of p63 motifs in dynamic enhancers underscores the key role of p63 in orchestrating the enhancer landscape during keratinocyte differentiation.

### Decreased Active Enhancers Associated with p63-Binding Deficiency in p63 Mutant Keratinocytes

Based on the DNA-binding deficiency of EEC mutants shown by various studies and the dominant-negative model, we expected to detect DNA-binding loss in p63 mutant keratinocytes. To characterize this and evaluate the effect of p63 mutations on the enhancer landscape, we performed p63 chromatin immunoprecipitation sequencing (ChIP-seq) using a p63 antibody that is not affected by mutations in the p63 DNA-binding domain (Figure S4A) (Shen et al., 2013) and H3K27ac ChIP-seq in all three p63 mutant keratinocytes. A total number of 33,366 p63-binding sites (p63 BSs) detected in both control and mutant keratinocytes were analyzed, and we observed globally reduced p63 binding signals in p63 mutant keratinocytes as compared to the control keratinocytes (Figure 3A; Tables S3A–S3E). It should be noted that no clear increased p63 binding or *de novo* p63 BSs were observed in p63 mutant keratinocytes. K-means clustering analysis showed that p63 BSs can be clustered into three groups based on the binding signals. Clusters p63-C1 and p63-C2 had decreased p63 binding to a lesser extent, whereas loci in p63-C3 showed more dramatic to almost complete loss of p63-binding signals (Figure 3A). The p63-binding pattern did not change much in mutant keratinocytes during differentiation (Figure S4D). Accordingly, the difference of H3K27ac signals at p63-C1 and p63-C2 between control and p63 mutant keratinocytes was not obvious, whereas a decrease of H3K27ac signals was detected at p63 C3 in p63 mutant keratinocytes (Figures 3A and S4B).

Using GREAT GO annotation to assess nearby genes, all three clusters of p63 BSs were significantly enriched for genes involved in epidermis development (Figure 3B). We also performed human phenotype analyses to investigate the disease significance of these p63 BSs, and the disease terms detected were mainly related to ectodermal dysplasia, such as plantar hyperkeratosis, nail dystrophy, and alopecia (Figure S4C). We further explored whether a specific molecular mechanism controls the discordant p63-binding losses. We examined whether the cooperation with different co-regulating TFs contributes to the differential p63-binding loss by motif scanning but did not find significant differential p63 co-regulators that can potentially cause the discordant p63-binding loss (Tables S3H–S3J). Next,

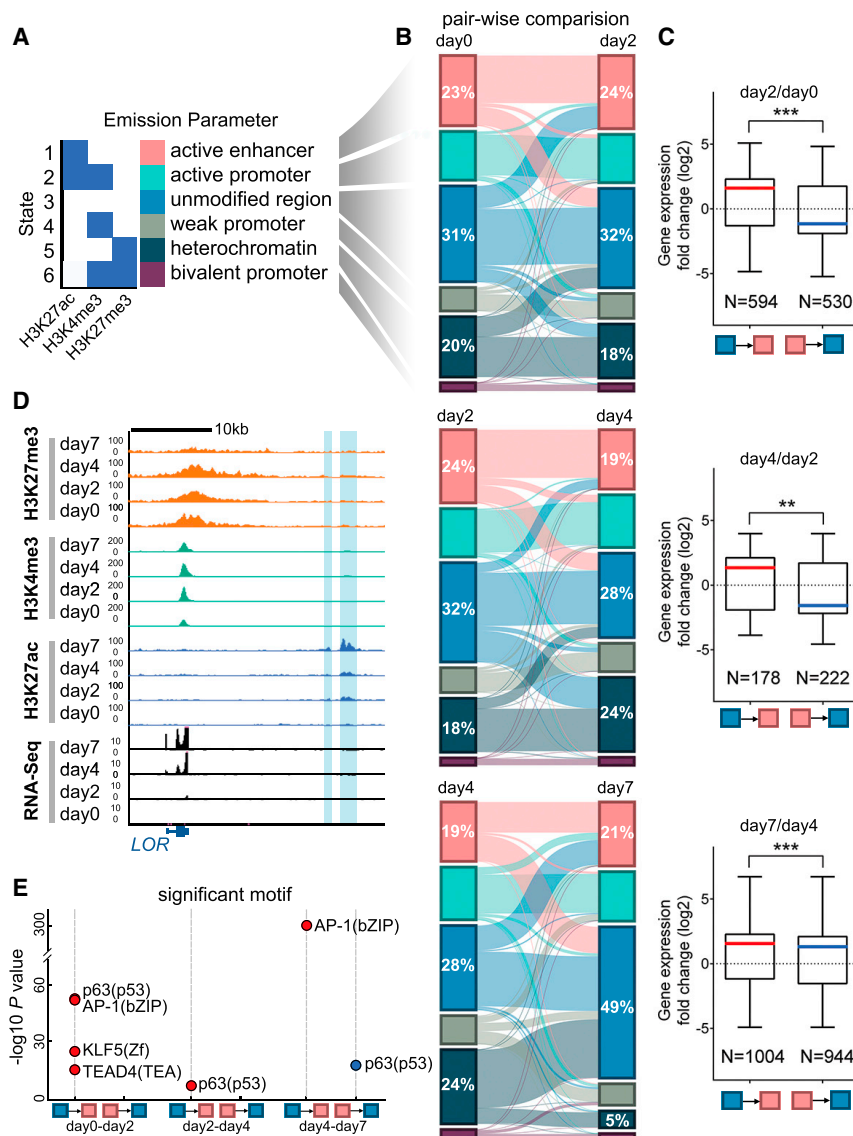


**Figure 2. Chromatin Dynamics during Control Keratinocyte Differentiation**

(A) Emission states of the ChromHMM hidden Markov model distinguishing six combinations defined by three histone modifications: H3K27ac, H3K4me3, and H3K27me3. “Unmodified regions” refers to genomic regions that do not have any of these modifications.

(B) Alluvial plots of pairwise chromatin state transitions during differentiation. The column height represents the percentage of each of the chromatin state relative to the sum of the six states. Genomic regions defined as unmodified regions at all differentiation stages were excluded in this analysis. The percentages of active enhancers, unmodified regions, and the heterochromatin are labeled.

(C) Pairwise comparison of differential gene expression (fold change) associated with genomic regions that shift between unmodified regions and active enhancers during differentiation, corresponding to (B). Data are shown as mean  $\pm$  SD; \*\* $p < 0.01$ , and \*\*\* $p < 0.001$ , unpaired t test.

(D) Chromatin state dynamics of unmodified regions and active enhancers during differentiation at the locus of *LOR*.

(E) Significantly enriched motifs in the dynamic enhancer regions. Red dots, motifs that were enriched in regions shifting from unmodified regions to active enhancers; blue dots, motifs that were enriched in regions shifting from active enhancers to unmodified regions.

See also Figure S3 and Table S2.

using our previously established p63scan algorithm (Kouwenhoven et al., 2010), we found that p63-C3 BSs sites had the lowest percentage of BSs with the p63 motif (85%) and the lowest average motif score (mean motif score of 8.3) compared to p63-C1 (98%; mean motif score of 9.5) and p63-C2 (93%; mean motif score of 8.8) BSs (Figure 3C; Tables S3K–S3N). Our observations thus suggest that p63 motif strength determines the selectivity of the loss of p63 binding.

Lastly, we examined whether gene deregulation was associated with impaired p63 binding. Genes near p63 BSs (all three [p63-C1, p63-C2, and p63-C3]) had a significantly larger proportion of deregulated genes (34.8%,  $p = 0$ , hypergeometric test) when compared to all annotated genes (12.5%) (Figure 3D; Table S3F). A significant difference in the percentage of deregulated genes was also found in genes associated with p63-C3 BSs (35.4%,  $p = 0$ , hypergeometric test) compared to all genes with p63 BSs (Table S3G). These data indicate

to gene deregulation and potentially contribute to ectodermal dysplasia phenotypes.

### Redistribution of Enhancers in p63 Mutant Keratinocytes

Although a significant percentage of deregulated genes (~54%) were associated with impaired p63 binding, a large number of deregulated genes did not seem to be directly regulated by p63. Furthermore, we observed many enhancers with unexpected increased H3K27ac signals near deregulated genes in p63 mutant keratinocytes (Figure 4A, blue shaded regions). Therefore, we compared H3K27ac between control and p63 mutant keratinocytes with MANorm (Shao et al., 2012). We identified 17,931 genomic regions that had significantly higher H3K27ac signals in mutant keratinocytes (referred to as mutant-specific enhancers), which is more than the 15,057 regions that had significantly higher H3K27ac in control

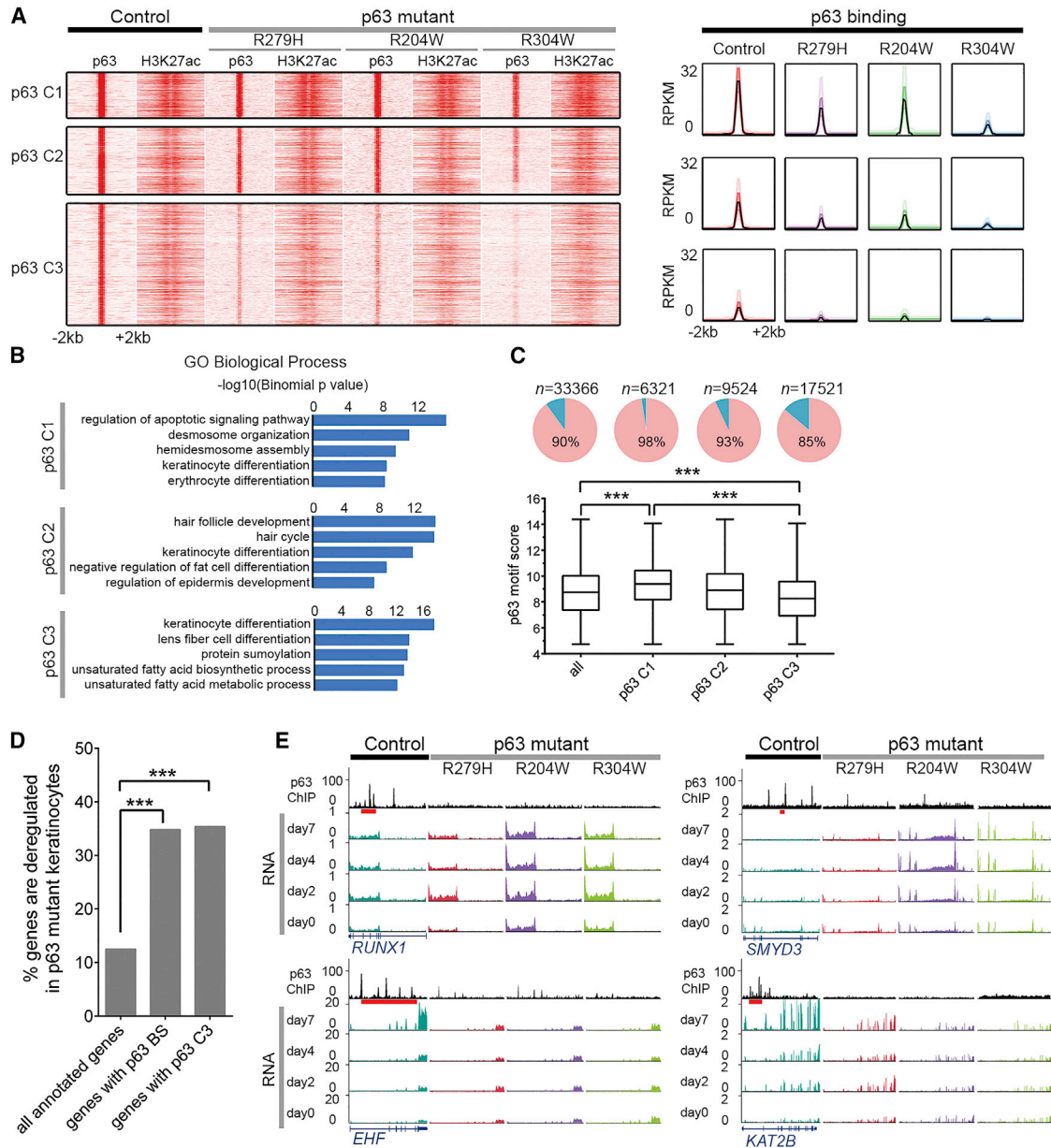


**Figure 3. Decreased Active Enhancers Associated with p63-Binding Deficiency**

(A) K-means clustering of p63-binding sites (BSs) that are merged from control and p63 mutant keratinocytes groups p63 BSs into 3 classes ( $k = 3$ , metric = Pearson). Heatmaps and band plots are shown in a 4-kb window with summits of p63 BSs in the middle. Color intensity in heatmaps represents normalized read counts. In the band plots, the median enrichment was visualized as the black line while 50% and 90% ranges were depicted in lighter color, respectively.

(B) GREAT-based GO biological process annotation of p63 BSs in each cluster.

(C) p63 motif strength determined the selectivity of the loss of p63 binding. Top: pie charts showing the percentage of p63 BSs with a p63 motif. Bottom: boxplot showing motif score distribution. Data are shown as mean  $\pm$  SD; \*\*\* $p < 0.001$ , one-way ANOVA.

(D) Percentage of deregulated genes associated with all p63 BSs and p63 BSs from p63-C3 (p63 C3) compared with all annotated genes. \*\*\* $p < 0.001$ , hypergeometric test.

(E) ChIP-seq of p63 and RNA-seq data at the *RUNX1*, *EHF*, *SMYD3*, and *KAT2B* loci in control and p63 mutant keratinocytes. Red bars represent p63 BSs that were lost or decreased in p63 mutant keratinocytes.

See also Figure S4 and Table S3.

keratinocytes (referred to as control-specific enhancers) (Figures S5A and S4B; Table S4). Two replicas of H3K27ac ChIP-seq in R304W mutant keratinocytes showed a high correlation

(Pearson correlation coefficient of 0.94; Figure S5B), demonstrating the high reproducibility of these datasets. To validate these findings, H3K27ac ChIP-qPCR was performed on three

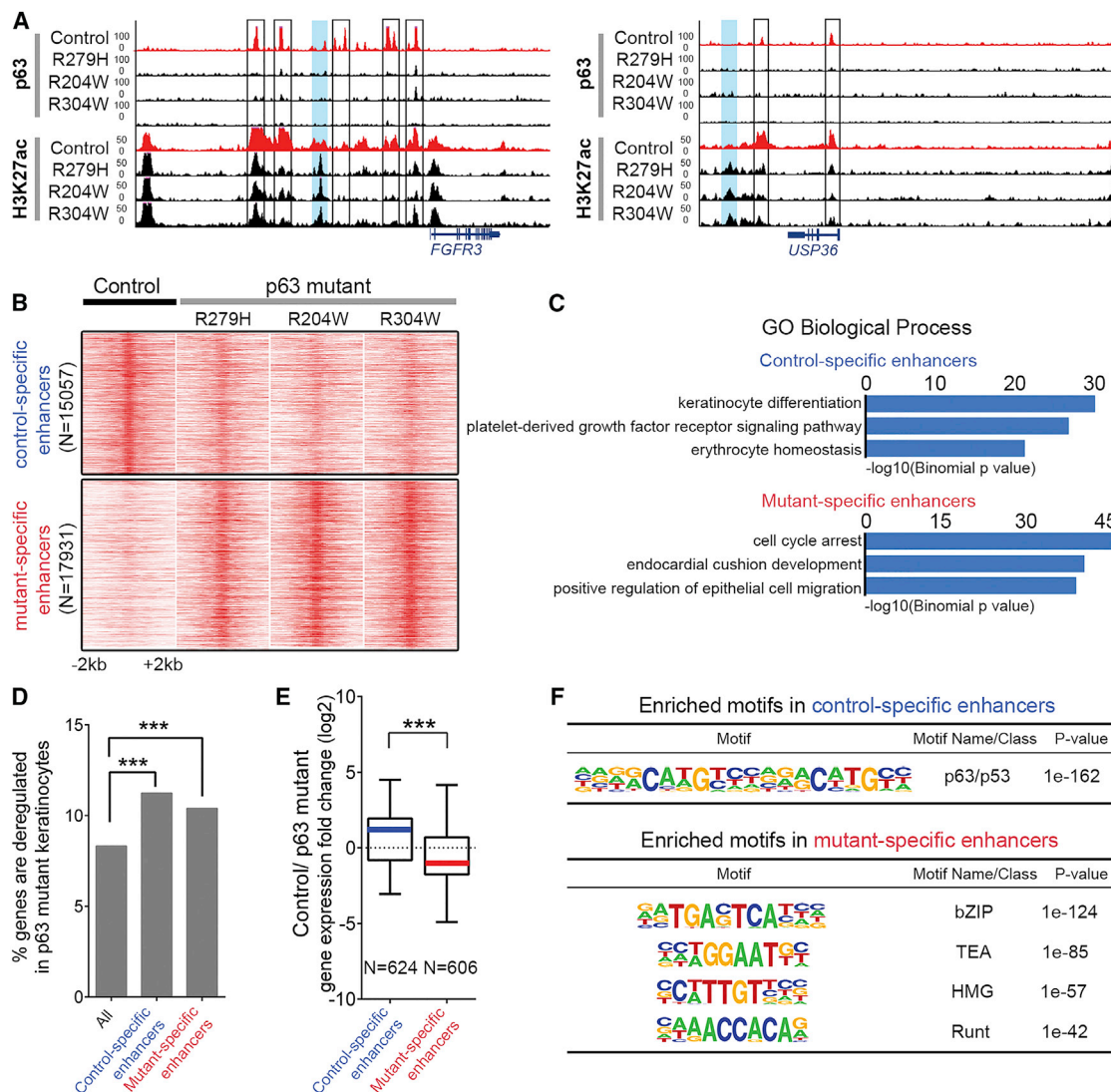


**Figure 4. Redistribution of Enhancers in p63 Mutant Keratinocytes**

(A) Examples of redistributed enhancers marked by H3K27ac signals between control and p63 mutant keratinocytes. Black boxes indicate lost p63 BS with lost or decreased H3K27ac signals. Blue shades indicate gained enhancers in p63 mutant keratinocytes.

(B) Heatmaps of differential H3K27ac peaks in control and p63 mutant keratinocytes shown in a 4-kb window with summits of H3K27ac peaks in the middle. Color intensity in heatmaps represents normalized read counts.

(C) GREAT-based GO biological process annotation of differential enhancers.

(D) Percentage of deregulated genes relative to all genes associated with active enhancers, all or control- or mutant-specific enhancers. \*\*\* $p < 0.001$ , hypergeometric test.

(E) Differential gene expression (fold change) associated with control or mutant-specific enhancers. Data are shown as mean  $\pm$  SD; \*\*\* $p < 0.001$ , unpaired t test.

(F) Highly enriched motifs found in control-specific or mutant-specific enhancers.

See also [Figure S5](#) and [Table S4](#).

control-specific and three mutant-specific enhancer loci ([Figure S5C](#)). Genes nearby control-specific enhancers were associated with keratinocyte differentiation, whereas those nearby mutant-specific enhancers were involved in cell-cycle regulation, migration, and non-epithelial processes ([Figure 4C](#)). Furthermore, a significantly larger proportion of deregulated genes had either control-specific or mutant-specific H3K27ac sites ([Figure 4D](#)). As expected, control-specific enhancers were associated with gene downregulation, whereas mutant-

specific enhancers were associated with gene upregulation in p63 mutant keratinocytes ([Figure 4E](#)). Taken together, the observed genome-wide redistribution of enhancers marked by H3K27ac indicates that epigenome rewiring occurs in p63 mutant keratinocytes.

To investigate the underlying mechanisms of enhancer re-distribution, a *de novo* motif scan was performed. We detected the p53 or p63 motif family as the top enriched motif among control-specific enhancers ([Figure 4F](#); [Table S4I](#)), consistent with the

impaired p63 binding and loss of active enhancers in p63 mutant keratinocytes (Figure 3A). In contrast, motif analyses of mutant-specific enhancers captured motifs of bZIP, TEA, high-mobility group (HMG), and Runt family TFs (Table S4M). These data suggest that aberrant recruitment of TFs induces gain of enhancers.

One scenario of aberrant recruitment of TFs may result from the abnormal upregulation of TFs in mutant keratinocytes. To assess this possibility, we examined differential expression of TFs. Among 1,581 examined TFs (Saeed et al., 2014), 106 and 103 TFs were down- and upregulated, respectively, in p63 mutant keratinocytes (Figure S6). Interestingly, most downregulated TFs had p63 BSs nearby and therefore are potential p63 direct targets. In contrast, fewer upregulated TFs had p63 BSs. To predict candidate TFs that are potentially bound to mutant-specific enhancers, we used two criteria: (1) TFs whose binding motifs were enriched in mutant-specific enhancers (Figure 4F), and (2) TFs that were upregulated in all three p63 mutant keratinocytes at the proliferation stage (day 0) (Figure S6A). Among TFs that were consistently upregulated in mutant keratinocytes, RUNX1 and SOX4 belong to the TF families whose motifs were enriched in mutant-specific enhancers. We performed qRT-PCR validation to confirm the higher expression of SOX4 in p63 mutant keratinocytes (Figure S6B). ChIP-qPCR of SOX4 also confirmed a number of SOX4 BSs with higher binding signals in R304W mutant keratinocytes compared to control keratinocytes (Figure S6C). Interestingly, one of the candidate TFs RUNX1 is a known p63 target (Masse et al., 2012) and a potential p63 co-regulator. RUNX1 had many lost p63 BSs in the gene locus and was consistently upregulated in p63 mutant keratinocytes (Figures 3E and S6A).

### Deregulated p63 and RUNX1 Cooperation Contributes to Transcriptional Rewiring in Mutant p63 Keratinocytes

To characterize p63 and RUNX1 co-regulation, we performed RUNX1 ChIP-seq in control keratinocytes. K-means clustering of RUNX1 BSs in combination with p63 binding and histone modification profiles showed that RUNX1 and p63 preferentially co-bound in active enhancer regions (Figure 5A). RUNX1 bound more frequently to active promoters marked by H3K4me3 (RUNX1-C4) than p63 (RUNX1-C1 and RUNX1-C3) (Figure 5A; Table S5A). Genes near the co-regulated enhancers (RUNX1-C1 and RUNX1-C3 [e.g., *ITGB1* and *EGFR*]) were mainly involved in epidermis development and programmed cell death, respectively (Figures 5B and 5C). The observed upregulation of RUNX1 expression (Figure 5D) and loss of p63 binding in the *RUNX1* gene body in p63 mutant keratinocytes (Figure 3E) indicated that deregulation of RUNX1 expression is probably due to loss of p63 control. To further confirm this, we performed small interfering RNA (siRNA) knockdown of p63 in control keratinocytes. Similar to the upregulated *RUNX1* expression in p63 mutant keratinocytes, *RUNX1* expression was significantly increased in p63 knockdown keratinocytes (Figure 5E).

To assess whether upregulated *RUNX1* expression leads to its aberrant recruitment to mutant-specific enhancers in p63 mutant keratinocytes, we compared RUNX1 binding in control keratinocytes and R304W mutant keratinocytes (Figure 6A; Tables S5B–S5D). Among all RUNX1 BSs, there were 7,918 RUNX1 BSs with higher binding signals and 7,898 sites with lower binding signals

in R304W mutant keratinocytes (Tables S5B–S5F). RUNX1 BSs with increased binding signals in R304W mutant keratinocytes were more often located in active enhancer regions accompanied by increased H3K27ac signals (Figure 6B; Table S5E), while those with decreased RUNX1-binding signals were more often located in promoter regions (Figures S7A and S7B; Table S5F).

To test whether increased RUNX1 expression is responsible for deregulating gene expression in p63 mutant keratinocytes, we performed RUNX1 knockdown in R304W mutant keratinocytes. As the proper RUNX1 expression level is important for cell proliferation (Hoi et al., 2010; Masse et al., 2012), we carefully titrated RUNX1 siRNA oligonucleotides to achieve a level of RUNX1 expression similar to that in control keratinocytes. RNA-seq analyses showed that the overall gene expression of siRUNX1-treated R304W mutant keratinocytes was more similar to that of control keratinocytes in PCA (Figure S7C). Among the 3,294 upregulated genes in R304W mutant keratinocytes, 276 genes were significantly rescued downregulated upon siRUNX1 (Figure 6C; Tables S5H and S5I), such as *KRT8* (Figure S7E). Many of the rescued genes were involved in adhesion and other non-epithelial functions, such as angiogenesis. Importantly, among the 3,187 downregulated genes in R304W mutant keratinocytes, 218 genes were significantly rescued, with upregulated expression upon siRUNX1 (Figure 6D; Tables S5J and S5K), such as *KRT1* and *HES5* (Figures 6E and S7D). Many of these genes are important for epidermal development and keratinocyte differentiation. The number of rescued genes was significantly higher than random expectations (276/3,294, hypergeometric test  $p < 7.272e-102$ ; 218/3,184, hypergeometric test  $p < 4.305e-54$ ). Partial but significant rescues by siRUNX1 were expected, as deregulated genes caused by loss of p63 binding in p63 mutant keratinocytes could not be rescued simply by RUNX1 knockdown. qRT-PCR and western blotting experiments validated rescued gene expression of *KRT1*, *SMYD3*, and *KRT18* in R304W mutant keratinocytes upon siRUNX1 (Figures 6F and 6G). To further investigate whether siRUNX1 can rescue the enhancer landscape in R304W mutant keratinocytes, we performed H3K27ac ChIP-seq in these cells. Indeed, we observed a clear decrease of H3K27ac signals at enhancers that had higher H3K27ac signals and bound by RUNX1 in p63 mutant keratinocytes (Figure 6B;  $n = 6,035$ ) in two biological replicas (Figures 6H and S7E), such as enhancers near *NRP1*, which is involved in angiogenesis (Figure 6I). Taken together, our data suggest that reversing upregulated *RUNX1* expression can rescue deregulated gene expression and the enhancer landscape in p63 mutant keratinocytes.

## DISCUSSION

The master regulator role of p63 in epidermal development has been established by many studies using *in vitro* and *in vivo* models. However, it remains unclear how p63 mutations affect the chromatin landscape and gene expression that contribute to diseases. In this study, we used EEC-patient-derived skin keratinocytes carrying heterozygous p63 DNA-binding domain mutations as the cellular model to characterize the global gene regulatory alteration. We showed that the epidermal cell identity was compromised in p63 mutant keratinocytes, as indicated by

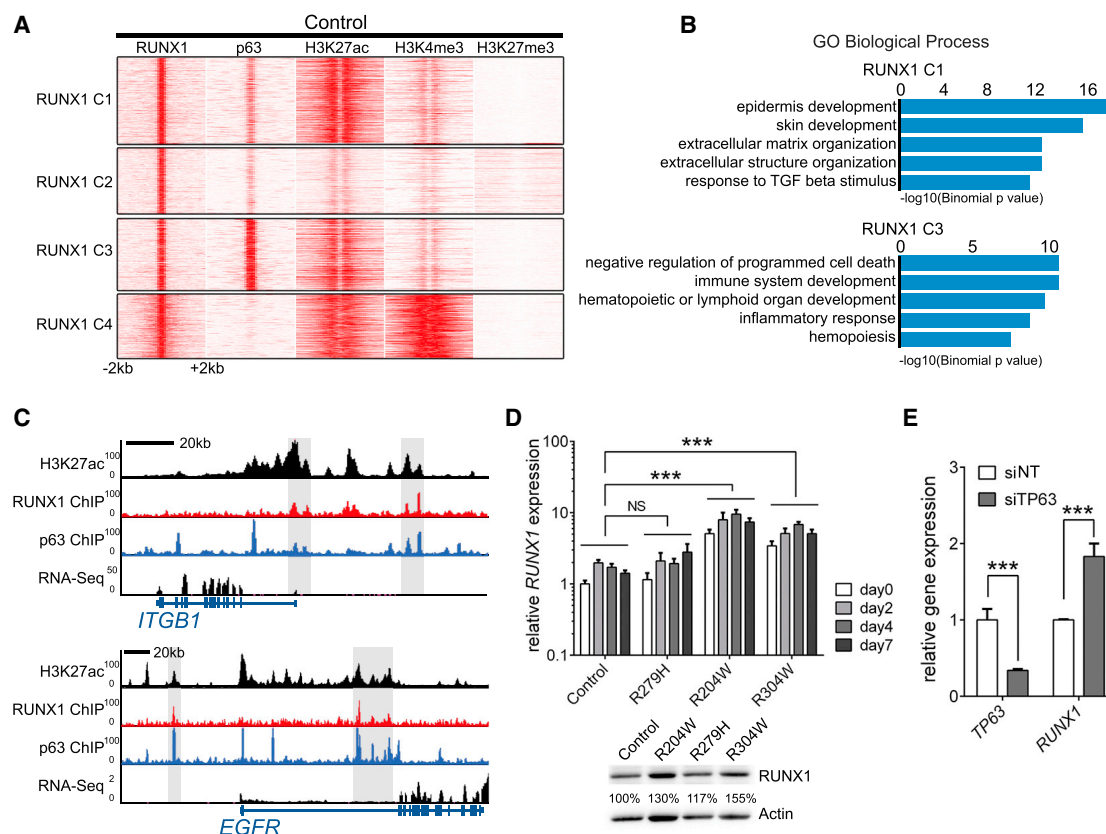


**Figure 5. RUNX1 Is a Co-regulator and Target Gene of p63**

(A) K-means clustering of RUNX1 BSs in control keratinocytes. RUNX1-binding signals are shown in heatmaps in a 4-kb window with summits of RUNX1 BSs in the middle ( $k = 4$ , metric = Pearson). Color intensity represents normalized read counts.

(B) GREAT-based GO biological process annotation of RUNX1 BSs in RUNX1 C1 and C3.

(C) Representative example of RUNX1 and p63-co-regulated genes *ITGB1* and *EGFR*.

(D) Validation of *RUNX1* gene expression by qRT-PCR and western blotting. In qRT-PCR analysis, relative gene expression was normalized to the reference gene *hARP*. Data are shown as mean  $\pm$  SD, technical replicates  $n = 2$ ; NS,  $p > 0.05$ ; \*\*\* $p < 0.001$ , two-way ANOVA. Actin was used as a loading control for the quantification of RUNX1 protein levels (shown as percentage) in western blotting.

(E) Gene expression analysis by qRT-PCR of *TP63* and *RUNX1* expression in *TP63* knockdown (siTP63) compared to non-targeting siRNA (siNT) in control keratinocytes. Gene expression was normalized to the reference gene *hARP*. Data are shown as mean  $\pm$  SD, technical replicates  $n = 2$ ; \*\*\* $p < 0.001$ , two-way ANOVA.

See also [Figure S6](#) and [Table S5](#).

downregulated epidermal genes and upregulated non-epithelial genes. In addition to loss of p63 binding leading to reduced p63-bound active enhancers, we unexpectedly observed abnormally induced active enhancers that were bound by upregulated p63 co-regulators such as RUNX1. Reversing RUNX1 upregulation in p63 mutant keratinocytes rescued a part of the deregulated gene expression and altered enhancer landscape. Our data suggest an intriguing model whereby rewiring of the enhancer landscape, contributed by both loss of p63-bound active enhancers and gain of active enhancers induced by overexpressed p63 co-regulators, gives rise to gene deregulation and phenotypes of EEC syndrome (Figure 7).

Many epidermal genes were downregulated in mutant keratinocytes, consolidating the key role of p63 in epidermal development. In addition, upregulated mesenchymal genes and neuronal genes in mutant keratinocytes (Figure 1D) suggest

that these cells have less defined epidermal cell fate. For example, mesodermal related genes such as *ACTA2* and *COL4A1*, which were upregulated during epidermal commitment of p63-depleted embryonic stem cells (Shalom-Feuerstein et al., 2011), were also upregulated in p63 mutant keratinocytes (Table S1E). In agreement, gene coexpression network analyses showed that the scattered upregulated genes involved in extracellular matrix organization were connected with two modules (keratinization and nucleosome assembly) associated with downregulated genes in mutant keratinocytes (Figure 1E). This suggests that gene expression in p63 mutant keratinocytes deviates from the proper epidermal cell fate to establish a new differentiation direction through chromatin remodeling processes. In addition to directly regulating chromatin remodeling factors (Figure S2B), we showed in this study that p63 motif was most significantly enriched in active enhancers at early differentiation

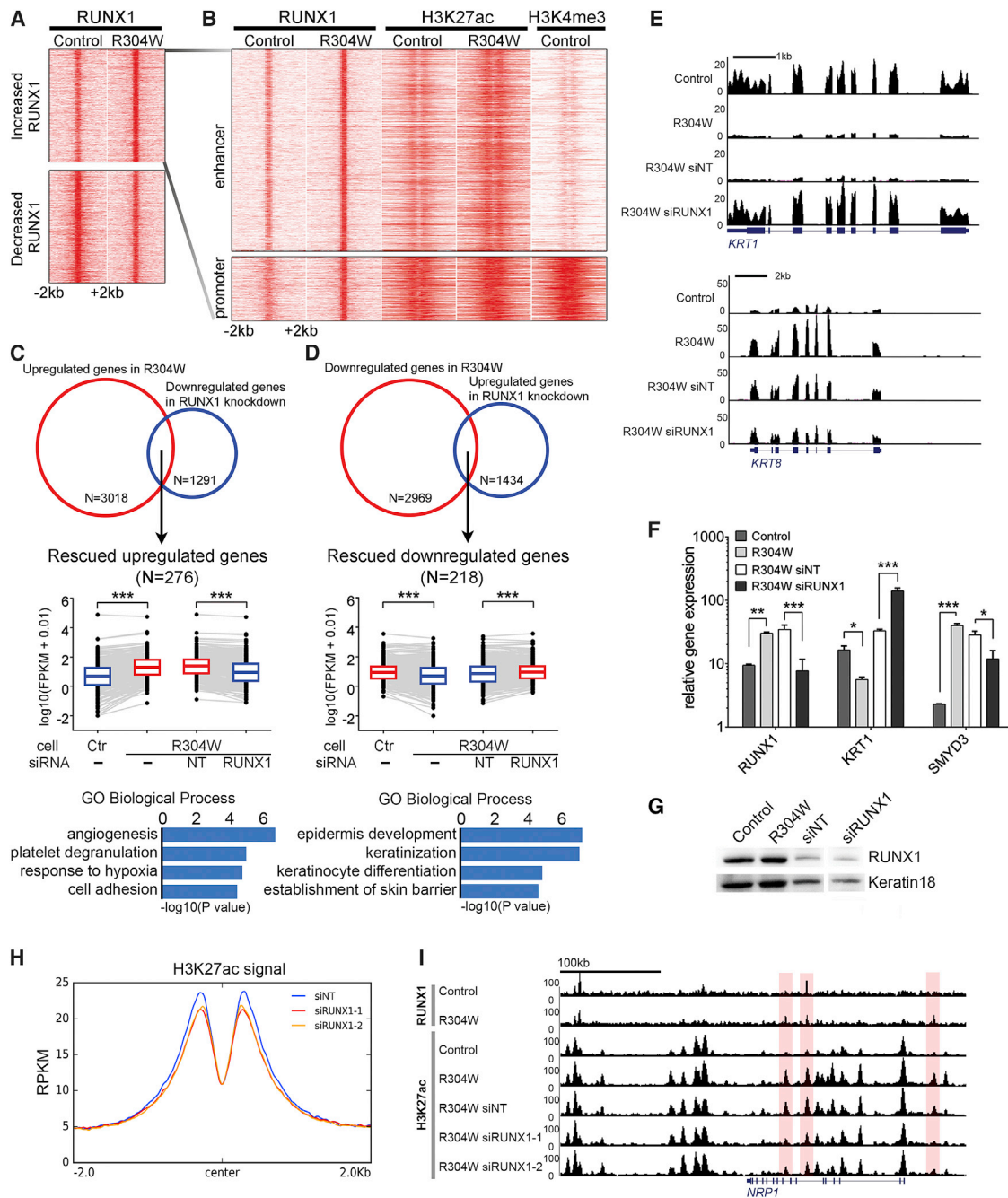


**Figure 6. Increased RUNX1 Binding Contributes to Gene Deregulation**

(A) K-means clustering of RUNX1 BSs from control and R304W mutant keratinocytes are shown in heatmaps in a 4-kb window with summits of merged RUNX1 BSs in the middle ( $k = 2$ , metric = Pearson). Color intensity represents normalized read counts.

(B) Zoom-in re-clustering of increased RUNX1 BSs in R304W mutant keratinocytes showing that the majority of RUNX1 BSs with increased signals are enhancers.

(C) 276 significantly upregulated genes in R304W mutant keratinocytes that were rescued with siRUNX1 ( $p < 0.05$ ). The significance of the overlap was calculated using a hypergeometric test ( $p < 7.272e-102$ ). Expression (RNA-seq FPKM) of rescued genes under different conditions is shown as mean  $\pm$  SD. \*\*\* $p < 0.001$ , t test. DAVID-based GO biological process annotation is shown at the bottom.

(D) 218 significantly downregulated genes in R304W mutant keratinocytes that were rescued with siRUNX1 ( $p < 0.05$ ). The significance of the overlap was calculated with hypergeometric test ( $p < 4.305e-54$ ).

(E) UCSC genome browser screenshots of RNA-seq data at the gene loci of *KRT1* and *KRT8* are shown as examples of rescued genes by siRUNX1.

(F) Gene expression analyses by qRT-PCR of *RUNX1*, *KRT1*, and *SMYD3*. Relative gene expression of these genes was normalized to the reference gene *hARP*. Data are shown as mean  $\pm$  SD, technical replicates  $n = 2$ ; \* $p < 0.1$ , \*\* $p < 0.01$ , \*\*\* $p < 0.001$ , two-way ANOVA.

(legend continued on next page)

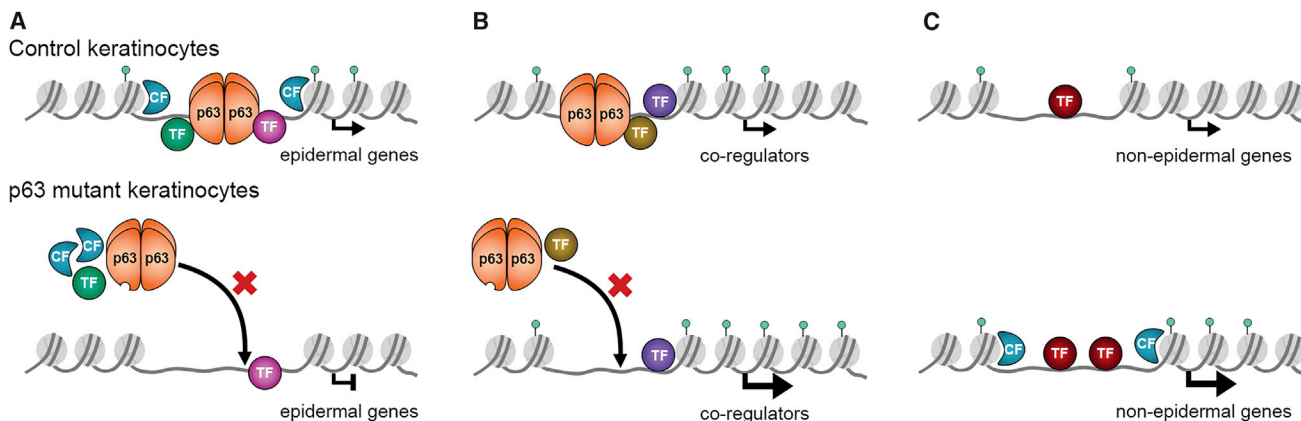


**Figure 7. Model of p63-Controlled Gene Regulation and Cell Identity in Control and p63 Mutant Keratinocytes**

(A) p63-mediated activation of epidermal genes. In control keratinocytes, p63 activates epidermal genes by binding to nearby active enhancers, in cooperation with co-regulating TFs and chromatin factors (CFs). In p63 mutant keratinocytes, mutant p63 cannot bind to these enhancers, which results in downregulation of epidermal genes.

(B) p63-mediated fine-tuning of its co-regulators. In control keratinocytes, p63 fine-tunes the expression of its co-regulators, such as RUNX1 and SOX4. In p63 mutant keratinocytes, mutant p63 cannot bind to these enhancers and loses fine-tuning control.

(C) Indirect activation of enhancers due to lack of p63 control. Overexpressed p63 co-regulators such as RUNX1 can bind to less controlled open chromatin regions and enhancers to activate non-epidermal genes in p63 mutant keratinocytes.

stages (Figure 2E). These results support the pivotal role of p63 in regulating enhancers to activate epidermal differentiation genes, especially at the initiation stage.

In addition to its activator role for epidermal genes, it has been shown that p63 can function as a repressor to repress p21 (*CDKN1A*) through recruiting histone deacetylase 1 (HDAC1) and HDAC2 (LeBoeuf et al., 2010; Ramsey et al., 2011). RUNX1, a co-regulator of p63, is regulated by p63 in a complex fashion. Depending on the differentiation state of keratinocytes, p63 activates or represses *RUNX1* expression (Masse et al., 2012). In our analyses, we detected upregulation of *RUNX1* in proliferating mutant keratinocytes (Figures 3E and 5D), consistent with the repressor role of p63 for these genes. However, p63-bound enhancers at the *RUNX1* locus were active enhancers, marked by H3K27ac, in contrast to classically defined repressed regions that are marked by H3K27me3 and H3K9me3. Furthermore, no H3K27me3 or H3K9me3 repression mark was found at any p63 BS (Kouwenhoven et al., 2015a), indicating that p63-bound enhancers are not repressed by polycomb- or heterochromatin-related mechanisms. To reconcile the apparent contradiction that p63 binds to active enhancers to repress gene expression, we speculate that p63 binds to these active enhancers to fine-tune expression of these genes by recruiting repressors such as HDACs. When p63 expression or function is compromised, such as in p63 mutant keratinocytes

or p63 knockdown cells (Figures 5D and 5E), the fine-tuning or repression mechanisms are relieved, and the expression of these genes is enhanced (Figure 7B).

In this study, we showed that p63-binding loss and loss of active enhancers occurs at a genome-wide scale in patient keratinocytes carrying heterozygous EEC mutations (Figure 3A). This indicates that the mutant p63 protein has a dominant-negative effect on DNA binding over the wild-type p63 that is also present in the cell, likely because the p63 protein is DNA-binding competent as a tetramer (Dötsch et al., 2010; Serber et al., 2002). These genome-wide findings corroborate the dominant-negative model of EEC p63 mutations that has been proposed by several previous studies using *in vitro* approaches and allele-specific knockdown of p63 mutant.

Unexpectedly, we observed a large number of gained active enhancers in all three p63 mutant keratinocytes (Figures 4A, 4B, and S5A). These mutant-specific enhancers were enriched for motifs of TFs that normally cooperate with p63 in keratinocytes (Figure 4F). Many of these TFs were deregulated in p63 mutant keratinocytes (Figure S6) and are direct p63 targets, such as RUNX1 (Figures 3E and 5D). This indicates that rewiring of the transcriptional program is caused not only by loss of p63-bound active enhancers but also by an indirect effect of altered expression of p63 co-regulating TFs. ChIP-seq analyses revealed an altered RUNX1-binding profile in p63 mutant

(G) Western blotting analysis of RUNX1 and KRT18 in control and R304W mutant keratinocytes and in R304W keratinocytes treated with siRNA oligos. The RUNX1 knockdown was tested with two siRUNX1 oligos. The informative siRUNX1 oligo resulted in approximately 50% knockdown of RUNX1 at the protein level in R304W keratinocytes, as compared to the non-targeting oligo (NT). The blot with the non-informative siRUNX1 oligo without clear RUNX1 knockdown is included in Table S6. The protein samples were first titrated by western blotting of Actin and equal amounts were loaded for RUNX1 and KRT18 analyses. All western blots of the complete experiment are labeled and shown in Table S6.

(H) Decreased H3K27ac signals upon siRUNX1 treatment at the enhancers that had higher signals in R304W mutant keratinocytes (enhancer regions in B).

(I) An UCSC genome browser screenshot at the gene locus of *NRP1*, to show rescued enhancers, highlighted in pink.

See also Figure S7 and Table S5.

keratinocytes (Figure 6A). The increased RUNX1 binding was associated with increased H3K27ac signals (Figure 6B). Intriguingly, reversing *RUNX1* expression upon siRUNX1 could partially rescue gene deregulation and the enhancer landscape (Figures 6C–6I), indicating that overexpression of *RUNX1* in mutant keratinocytes contributes to gene deregulation and is at least partially responsible for the differentiation defects. Therefore, mutations in the p63 DNA-binding domain can give rise to an indirect gain-of-function effect by inducing aberrant binding of deregulated TFs to genome-wide enhancers (Figure 7C).

It should be noted that this gain-of-function model of p63 EEC mutations is different from the gain-of-function mechanism of a p63 mutation leading to phenotypically distinct Acro-dermatoungual-lacrimal-tooth (ADULT) syndrome (Rinne et al., 2007) and p53 mutations that give rise to cancers. It has been shown that some p53 mutants involved in cancer cannot bind to bona fide p53 targets, but cooperate with normal p53 co-regulators and bind to ectopic genomic sites to activate abnormal gene expression (Zhou et al., 2014; Zhu et al., 2015), a classical paradigm of gain of function. The most apparent difference between p53 and p63 EEC mutations is that EEC mutant p63 does not seemingly bind to ectopic genomic loci, as we did not observe any novel p63 BS in mutant keratinocytes (Figure 3A). The indirect gain-of-function action of p63 mutations is due to the overexpression of p63-co-regulating TFs, such as RUNX1, and their aberrant recruitment to mutant-specific enhancers.

In the siRUNX1 experiment, we did not expect a full rescue in p63 mutant keratinocytes, as p63-binding loss could not simply be rescued by *RUNX1* downregulation. With the same rationale, we also do not expect that overexpression of *RUNX1* would fully mimic p63 mutant keratinocyte phenotypes. However, it would be interesting to test whether overexpression of *RUNX1* in control keratinocytes can induce any differentiation defects. Furthermore, it is also of interest to further test the effect of other overexpressed p63 co-regulators such as TFs of the bZIP, TEA, and HMG families (SOX4) (Figure 4F) in the EEC disease mechanism. It is conceivable that knockdown of multiple such overexpressed TFs may rescue differentiation defects of p63 mutant keratinocytes to a better extent.

In conclusion, we identified a rewired enhancer landscape as a common mechanism in EEC p63 mutant keratinocytes. The enhancer rewiring includes loss of p63-bound active enhancers that regulate epidermal genes (Figure 7A) and gain of enhancers bound by overexpressed TFs that are normally fine-tuned by p63 (Figures 7B and 7C). It is conceivable that in EEC p63 mutant keratinocytes, the chromatin environment is less tightly controlled, and deregulated TFs can therefore bind to more exposed enhancers. The rewired enhancer landscape gives rise to gene deregulation that contributes to the less-defined epidermal cell fate and skin phenotypes of the disease. Taken together, enhancer landscape rewiring contributes to the disease mechanism of p63 mutation and may be common to many other diseases.

## STAR★METHODS

Detailed methods are provided in the online version of this paper and include the following:

- KEY RESOURCES TABLE
- CONTACT FOR REAGENT AND RESOURCE SHARING
- EXPERIMENTAL MODEL AND SUBJECT DETAILS
  - Human primary keratinocyte
- METHOD DETAILS
  - Cell culture
  - RNA extraction and quantitative real-time reverse transcription PCR (RT-qPCR)
  - Western blotting
  - RNA-seq and analysis pipeline
  - ChIP-seq and analysis pipeline
  - ChomHMM analysis
  - Motif analysis
  - siRNA nucleofection
- QUANTIFICATION AND STATISTICAL ANALYSIS
- DATA AND SOFTWARE AVAILABILITY

## SUPPLEMENTAL INFORMATION

Supplemental Information includes seven figures and six tables and can be found with this article online at <https://doi.org/10.1016/j.celrep.2018.11.039>.

## ACKNOWLEDGMENTS

We thank Gert Jan Veenstra for discussions and suggestions on the project. We thank Georgios Georgiou, Thomas te Wierik, and Guoqiang Yi for their help with data analyses, Hanna Niehues and Gijs. A.C. Franken for providing technical support of experiments, and Eva Janssen-Megens, Siebe van Gensen, and Rita Bylsma for operating the Illumina analyzer. We thank the ENCODE Consortium for sharing their data. This research was supported by the Netherlands Organisation for Scientific Research (grant NWO/ALW/MEERVOUD/836.12.010 to H.Z.), Radboud University (a fellowship to H.Z.), and the Chinese Scholarship Council (grant 201406330059 to J.Q.).

## AUTHOR CONTRIBUTIONS

J.Q. and H.Z. conceived and designed the experiments. J.Q., S.E.J.T., J.P.H.S., E.N.K., M.O., C.L., H.G.S., H.v.B., K.W.M., and H.Z. wrote and revised the manuscript. J.Q., S.E.J.T., J.P.H.S., E.N.K., and E.H.v.d.B. performed the experiments. J.Q., M.O., and H.Z. analyzed the data.

## DECLARATION OF INTERESTS

The authors declare no competing interests.

Received: May 1, 2017  
 Revised: September 16, 2018  
 Accepted: November 8, 2018  
 Published: December 18, 2018

## REFERENCES

- Bao, X., Rubin, A.J., Qu, K., Zhang, J., Giresi, P.G., Chang, H.Y., and Khavari, P.A. (2015). A novel ATAC-seq approach reveals lineage-specific reinforcement of the open chromatin landscape via cooperation between BAF and p63. *Genome Biol.* 16, 284.
- Browne, G., Cipollone, R., Lena, A.M., Serra, V., Zhou, H., van Bokhoven, H., Dötsch, V., Merico, D., Mantovani, R., Terrinoni, A., et al. (2011). Differential altered stability and transcriptional activity of  $\Delta$ Np63 mutants in distinct ectodermal dysplasias. *J. Cell Sci.* 124, 2200–2207.
- Brunner, H.G., Hamel, B.C., and Van Bokhoven, H. (2002). The p63 gene in EEC and other syndromes. *J. Med. Genet.* 39, 377–381.

- Candi, E., Dinsdale, D., Rufini, A., Salomoni, P., Knight, R.A., Mueller, M., Krammer, P.H., and Melino, G. (2007). Tap63 and DeltaNp63 in cancer and epidermal development. *Cell Cycle* 6, 274–285.
- Candi, E., Cipollone, R., Rivetti di Val Cervo, P., Gonfloni, S., Melino, G., and Knight, R. (2008). p63 in epithelial development. *Cell. Mol. Life Sci.* 65, 3126–3133.
- Celli, J., Duijf, P., Hamel, B.C., Bamshad, M., Kramer, B., Smits, A.P., Newbury-Ecob, R., Hennekam, R.C., Van Buggenhout, G., van Haeringen, A., et al. (1999). Heterozygous germline mutations in the p53 homolog p63 are the cause of EEC syndrome. *Cell* 99, 143–153.
- Dennis, G., Jr., Sherman, B.T., Hosack, D.A., Yang, J., Gao, W., Lane, H.C., and Lempicki, R.A. (2003). DAVID: Database for Annotation, Visualization, and Integrated Discovery. *Genome Biol.* 4, 3.
- Dobin, A., Davis, C.A., Schlesinger, F., Drenkow, J., Zaleski, C., Jha, S., Batut, P., Chaisson, M., and Gingeras, T.R. (2013). STAR: ultrafast universal RNA-seq aligner. *Bioinformatics* 29, 15–21.
- Dötsch, V., Bernassola, F., Coutandin, D., Candi, E., and Melino, G. (2010). p63 and p73, the ancestors of p53. *Cold Spring Harb. Perspect. Biol.* 2, a004887.
- Ernst, J., and Kellis, M. (2012). ChromHMM: automating chromatin-state discovery and characterization. *Nat. Methods* 9, 215–216.
- Fessing, M.Y., Mardaryev, A.N., Gdula, M.R., Sharov, A.A., Sharova, T.Y., Rapisarda, V., Gordon, K.B., Smorodchenko, A.D., Poterlowicz, K., Ferone, G., et al. (2011). p63 regulates Satb1 to control tissue-specific chromatin remodeling during development of the epidermis. *J. Cell Biol.* 194, 825–839.
- Georgiou, G., and van Heeringen, S.J. (2016). fluff: exploratory analysis and visualization of high-throughput sequencing data. *PeerJ* 4, e2209.
- Hoi, C.S., Lee, S.E., Lu, S.-Y., McDermitt, D.J., Osorio, K.M., Piskun, C.M., Peters, R.M., Paus, R., and Tumber, T. (2010). Runx1 directly promotes proliferation of hair follicle stem cells and epithelial tumor formation in mouse skin. *Mol. Cell. Biol.* 30, 2518–2536.
- Huang da, W., Sherman, B.T., and Lempicki, R.A. (2009). Systematic and integrative analysis of large gene lists using DAVID bioinformatics resources. *Nat. Protoc.* 4, 44–57.
- Ihrig, R.A., Marques, M.R., Nguyen, B.T., Horner, J.S., Papazoglu, C., Bronson, R.T., Mills, A.A., and Attardi, L.D. (2005). Perp is a p63-regulated gene essential for epithelial integrity. *Cell* 120, 843–856.
- Kouwenhoven, E.N., van Heeringen, S.J., Tena, J.J., Oti, M., Dutilh, B.E., Alonso, M.E., de la Calle-Mustienes, E., Smeenk, L., Rinne, T., Parsaulian, L., et al. (2010). Genome-wide profiling of p63 DNA-binding sites identifies an element that regulates gene expression during limb development in the 7q21 SHFM1 locus. *PLoS Genet.* 6, e1001065.
- Kouwenhoven, E.N., Oti, M., Niehues, H., van Heeringen, S.J., Schalkwijk, J., Stunnenberg, H.G., van Bokhoven, H., and Zhou, H. (2015a). Transcription factor p63 bookmarks and regulates dynamic enhancers during epidermal differentiation. *EMBO Rep.* 16, 863–878.
- Kouwenhoven, E.N., van Bokhoven, H., and Zhou, H. (2015b). Gene regulatory mechanisms orchestrated by p63 in epithelial development and related disorders. *Biochim. Biophys. Acta* 1849, 590–600.
- Langfelder, P., and Horvath, S. (2008). WGCNA: an R package for weighted correlation network analysis. *BMC Bioinformatics* 9, 559.
- LeBoeuf, M., Terrell, A., Trivedi, S., Sinha, S., Epstein, J.A., Olson, E.N., Morrissey, E.E., and Millar, S.E. (2010). Hdac1 and Hdac2 act redundantly to control p63 and p53 functions in epidermal progenitor cells. *Dev. Cell* 19, 807–818.
- Li, H., and Durbin, R. (2009). Fast and accurate short read alignment with Burrows-Wheeler transform. *Bioinformatics* 25, 1754–1760.
- Livak, K.J., and Schmittgen, T.D. (2001). Analysis of relative gene expression data using real-time quantitative PCR and the 2(-Delta Delta C(T)) Method. *Methods* 25, 402–408.
- Love, M.I., Huber, W., and Anders, S. (2014). Moderated estimation of fold change and dispersion for RNA-seq data with DESeq2. *Genome Biol.* 15, 550.
- Mardaryev, A.N., Gdula, M.R., Yarker, J.L., Emelianov, V.U., Poterlowicz, K., Sharov, A.A., Sharova, T.Y., Scarpa, J.A., Joffe, B., Solovei, I., et al. (2014). p63 and Brg1 control developmentally regulated higher-order chromatin remodelling at the epidermal differentiation complex locus in epidermal progenitor cells. *Development* 141, 101–111.
- Masse, I., Barbolat-Boutrand, L., Molina, M., Berthier-Vergnes, O., Joly-Tonetti, N., Martin, M.T., Caron de Fromental, C., Kanitakis, J., and Lamartine, J. (2012). Functional interplay between p63 and p53 controls RUNX1 function in the transition from proliferation to differentiation in human keratinocytes. *Cell Death Dis.* 3, e318.
- McLean, C.Y., Bristor, D., Hiller, M., Clarke, S.L., Schaar, B.T., Lowe, C.B., Wenger, A.M., and Bejerano, G. (2010). GREAT improves functional interpretation of cis-regulatory regions. *Nat. Biotechnol.* 28, 495–501.
- Mills, A.A., Zheng, B., Wang, X.J., Vogel, H., Roop, D.R., and Bradley, A. (1999). p63 is a p53 homologue required for limb and epidermal morphogenesis. *Nature* 398, 708–713.
- Mulder, K.W., Wang, X., Escriu, C., Ito, Y., Schwarz, R.F., Gillis, J., Sirokmány, G., Donati, G., Uribe-Lewis, S., Pavlidis, P., et al. (2012). Diverse epigenetic strategies interact to control epidermal differentiation. *Nat. Cell Biol.* 14, 753–763.
- Novakovic, B., Habibi, E., Wang, S.-Y., Arts, R.J., Davar, R., Megchelenbrink, W., Kim, B., Kuznetsova, T., Kox, M., and Zwaag, J. (2016).  $\beta$ -glucan reverses the epigenetic state of LPS-induced immunological tolerance. *Cell* 167, 1354–1368.e1314.
- Ramírez, F., Dündar, F., Diehl, S., Grüning, B.A., and Manke, T. (2014). deepTools: a flexible platform for exploring deep-sequencing data. *Nucleic Acids Res.* 42, W187–91.
- Ramsey, M.R., He, L., Forster, N., Ory, B., and Ellisen, L.W. (2011). Physical association of HDAC1 and HDAC2 with p63 mediates transcriptional repression and tumor maintenance in squamous cell carcinoma. *Cancer Res* 71, 4373–4379.
- Rheinwald, J.G., and Green, H. (1977). Epidermal growth factor and the multiplication of cultured human epidermal keratinocytes. *Nature* 265, 421–424.
- Rinaldi, L., Datta, D., Serrat, J., Morey, L., Solanas, G., Avgustinova, A., Blanco, E., Pons, J.I., Matallanas, D., Von Kriegsheim, A., et al. (2016). Dnmt3a and Dnmt3b associate with enhancers to regulate human epidermal stem cell homeostasis. *Cell Stem Cell* 19, 491–501.
- Rinne, T., Brunner, H.G., and van Bokhoven, H. (2007). p63-associated disorders. *Cell Cycle* 6, 262–268.
- Romano, R.A., Birkaya, B., and Sinha, S. (2007). A functional enhancer of keratin14 is a direct transcriptional target of deltaNp63. *J. Invest. Dermatol.* 127, 1175–1186.
- Saeed, S., Quintin, J., Kerstens, H.H., Rao, N.A., Aghajani-farah, A., Matarese, F., Cheng, S.C., Ratter, J., Berentsen, K., van der Ent, M.A., et al. (2014). Epigenetic programming of monocyte-to-macrophage differentiation and trained innate immunity. *Science* 345, 1251086.
- Serber, Z., Lai, H.C., Yang, A., Ou, H.D., Sigal, M.S., Kelly, A.E., Darimont, B.D., Duijf, P.H., Van Bokhoven, H., McKeon, F., and Dötsch, V. (2002). A C-terminal inhibitory domain controls the activity of p63 by an intramolecular mechanism. *Mol. Cell. Biol.* 22, 8601–8611.
- Shalom-Fuerstein, R., Lena, A.M., Zhou, H., De La Forest Divonne, S., Van Bokhoven, H., Candi, E., Melino, G., and Aberdam, D. (2011).  $\Delta$ Np63 is an ectodermal gatekeeper of epidermal morphogenesis. *Cell Death Differ.* 18, 887–896.
- Shao, Z., Zhang, Y., Yuan, G.C., Orkin, S.H., and Waxman, D.J. (2012). MAnorm: a robust model for quantitative comparison of ChIP-Seq data sets. *Genome Biol.* 13, R16.
- Shen, J., van den Bogaard, E.H., Kouwenhoven, E.N., Bykov, V.J., Rinne, T., Zhang, Q., Tjallingii, G.S., Gilissen, C., van Heeringen, S.J., Schalkwijk, J., et al. (2013). APR-246/PRIMA-1(MET) rescues epidermal differentiation in

- skin keratinocytes derived from EEC syndrome patients with p63 mutations. *Proc. Natl. Acad. Sci. USA* 110, 2157–2162.
- Smoot, M.E., Ono, K., Ruscheinski, J., Wang, P.-L., and Ideker, T. (2011). Cytoscape 2.8: new features for data integration and network visualization. *Bioinformatics* 27, 431–432.
- Truong, A.B., Kretz, M., Ridky, T.W., Kimmel, R., and Khavari, P.A. (2006). p63 regulates proliferation and differentiation of developmentally mature keratinocytes. *Genes Dev.* 20, 3185–3197.
- van Bokhoven, H., and Brunner, H.G. (2002). Splitting p63. *Am. J. Hum. Genet.* 71, 1–13.
- van Bokhoven, H., Hamel, B.C., Bamshad, M., Sangiorgi, E., Gurrieri, F., Duijff, P.H., Vanmolkot, K.R., van Beusekom, E., van Beersum, S.E., Celli, J., et al. (2001). p63 gene mutations in EEC syndrome, limb-mammary syndrome, and isolated split hand-split foot malformation suggest a genotype-phenotype correlation. *Am. J. Hum. Genet.* 69, 481–492.
- Van Ruissen, F., de Jongh, G.J., Zeeuwen, P.L., Van Erp, P.E., Madsen, P., and Schalkwijk, J. (1996). Induction of normal and psoriatic phenotypes in sub-merged keratinocyte cultures. *J. Cell. Physiol.* 168, 442–452.
- Vernersson Lindahl, E., Garcia, E.L., and Mills, A.A. (2013). An allelic series of Trp63 mutations defines TAp63 as a modifier of EEC syndrome. *Am. J. Med. Genet. A.* 161A, 1961–1971.
- Yang, A., Schweitzer, R., Sun, D., Kaghad, M., Walker, N., Bronson, R.T., Tabin, C., Sharpe, A., Caput, D., Crum, C., and McKeon, F. (1999). p63 is essential for regenerative proliferation in limb, craniofacial and epithelial development. *Nature* 398, 714–718.
- Zhang, Y., Liu, T., Meyer, C.A., Eeckhoute, J., Johnson, D.S., Bernstein, B.E., Nusbaum, C., Myers, R.M., Brown, M., Li, W., and Liu, X.S. (2008). Model-based analysis of ChIP-seq (MACS). *Genome Biol.* 9, R137.
- Zhou, G., Wang, J., Zhao, M., Xie, T.-X., Tanaka, N., Sano, D., Patel, A.A., Ward, A.M., Sandulache, V.C., Jasser, S.A., et al. (2014). Gain-of-function mutant p53 promotes cell growth and cancer cell metabolism via inhibition of AMPK activation. *Mol. Cell* 54, 960–974.
- Zhu, J., Sammons, M.A., Donahue, G., Dou, Z., Vedadi, M., Getlik, M., Barsyte-Lovejoy, D., Al-awar, R., Katona, B.W., Shilatifard, A., et al. (2015). Gain-of-function p53 mutants co-opt chromatin pathways to drive cancer growth. *Nature* 525, 206–211.

## STAR★METHODS

### KEY RESOURCES TABLE

REAGENT or RESOURCE	SOURCE	IDENTIFIER
<b>Antibodies</b>		
Anti- $\beta$ -Actin antibody, Mouse monoclonal	Sigma-Aldrich	Cat#A1978, clone AC-15
Anti-LOR	Babco COVANCE	Cat#PRB-145P
Anti-RUNX1	Abcam	Cat#ab23980; RRID:AB_2184205
Anti-K18	Merck	Cat#MAB3234
Anti-H3K27ac	Diagenode	Cat#C15410174; RRID:AB_2716835
Anti-H3K4me3	Diagenode	Cat#C15410003
Anti-H3K27me3	Diagenode	Cat#C15410069
Anti-p63	Santa Cruz	Cat#H129
<b>Chemicals, Peptides, and Recombinant Proteins</b>		
Keratinocyte Basal Medium	Lonza	Cat#CC-4131
Penicillin/Streptomycin	GIBCO Life Technology	Cat#15140122
ethanolamine	Sigma Aldrich	Cat#141-43-5
O-phosphoethanolamine	Sigma Aldrich	Cat#1071-23-4
BPE(bovine pituitary extract)	Lonza	Cat#CC-4131
hydrocortisone	Lonza	Cat#CC-4131
insulin	Lonza	Cat#CC-4131
EGF(epidermal growth factor)	Lonza	Cat#CC-4131
USER enzyme	BioLab	Cat#M5505L
<b>Critical Commercial Assays</b>		
NucleoSpin RNA kit	MACHEREY-NAGEL	Cat#740955.250
iScript cDNA synthesis kit	Bio-Rad	Cat#170-8891
iQ SYBR® Green Supermix	Bio-Rad	Cat#1708887
MinElute Reaction Cleanup Kit	QIAGEN	Cat#28206
KAPA Hyper Prep Kit	Kapa Biosystems	Cat#KK8504
KAPA Library Quantification Kit	Kapa Biosystems	Cat#KK4844
<b>Deposited Data</b>		
Raw and analyzed data from control keratinocytes	This paper	GEO accession GSE98483
Raw and analyzed data from EEC keratinocytes	This paper	dbGaP accession ID phs001737.v1.p1
<b>Oligonucleotides</b>		
RT-qPCR primers	Biolegio BV, Nijmegen, the Netherlands	Provided in <a href="#">Table S1C</a>
siRNA	Thermo Fisher scientific	Provided in <a href="#">Table S5G</a>
<b>Software and Algorithms</b>		
STAR 2.5.0	<a href="#">Dobin et al., 2013</a>	<a href="https://github.com/alexdobin/STAR">https://github.com/alexdobin/STAR</a>
DESeq2	<a href="#">Love et al., 2014</a>	<a href="https://bioconductor.org/packages/release/bioc/html/DESeq2.html">https://bioconductor.org/packages/release/bioc/html/DESeq2.html</a>
WGCNA	<a href="#">Langfelder and Horvath, 2008</a>	<a href="https://horvath.genetics.ucla.edu/html/CoexpressionNetwork/Rpackages/WGCNA/">https://horvath.genetics.ucla.edu/html/CoexpressionNetwork/Rpackages/WGCNA/</a>
Cytoscape	<a href="#">Smoot et al., 2011</a>	<a href="https://cytoscape.org/">https://cytoscape.org/</a>
BWA	<a href="#">Li and Durbin, 2009</a>	<a href="http://bio-bwa.sourceforge.net/bwa.shtml">http://bio-bwa.sourceforge.net/bwa.shtml</a>
MACS2	<a href="#">Zhang et al., 2008</a>	<a href="https://github.com/taoliu/MACS">https://github.com/taoliu/MACS</a>
MANorm	<a href="#">Shao et al., 2012</a>	<a href="https://manorm.readthedocs.io/en/latest/">https://manorm.readthedocs.io/en/latest/</a>
fluff	<a href="#">Georgiou and van Heeringen, 2016</a>	<a href="https://fluff.readthedocs.io/en/latest/usage.html">https://fluff.readthedocs.io/en/latest/usage.html</a>

(Continued on next page)

**Continued**

REAGENT or RESOURCE	SOURCE	IDENTIFIER
deepTools	Ramírez et al., 2014	<a href="https://deeptools.readthedocs.io/en/develop/">https://deeptools.readthedocs.io/en/develop/</a>
ChromHMM	Ernst and Kellis, 2012	<a href="http://compbio.mit.edu/ChromHMM/">http://compbio.mit.edu/ChromHMM/</a>
p63scan	Kouwenhoven et al., 2010	N/A
HOMER	N/A	<a href="http://homer.ucsd.edu/homer/motif/">http://homer.ucsd.edu/homer/motif/</a>
GraphPad Prism	N/A	<a href="https://www.graphpad.com/scientific-software/prism/">https://www.graphpad.com/scientific-software/prism/</a>
Other		
Primer3	N/A	<a href="http://bioinfo.ut.ee/primer3-0.4.0/">http://bioinfo.ut.ee/primer3-0.4.0/</a>
DAVID	Huang da et al., 2009	<a href="https://david.ncifcrf.gov/">https://david.ncifcrf.gov/</a>
GREAT	McLean et al., 2010	<a href="http://great.stanford.edu/public/html/index.php">http://great.stanford.edu/public/html/index.php</a>
Sankey diagrams	N/A	<a href="http://sankeymatic.com/">http://sankeymatic.com/</a>
GeneProf	N/A	<a href="https://bio.tools/geneprof">https://bio.tools/geneprof</a>

**CONTACT FOR REAGENT AND RESOURCE SHARING**

Further information and requests for resources and reagents should be directed to and will be fulfilled by the Lead Contact, Huiqing Zhou ([j.zhou@science.ru.nl](mailto:j.zhou@science.ru.nl); [jo.zhou@radboudumc.nl](mailto:jo.zhou@radboudumc.nl)).

**EXPERIMENTAL MODEL AND SUBJECT DETAILS****Human primary keratinocyte**

All procedures for establishing and maintaining human primary keratinocytes were approved by the ethical committee of the Radboud university medical center (“Commissie Mensgebonden Onderzoek Arnhem-Nijmegen”). Informed consent was obtained from all donors of a skin biopsy. Primary keratinocytes were established previously from skin biopsies of three EEC syndrome patients carrying heterozygous mutations in the p63 DNA-binding domain, R204W (van Bokhoven et al., 2001), R279H (van Bokhoven and Brunner, 2002), and R304W (Celli et al., 1999), as well as of two healthy volunteers (Dombi23 and PCK19, referred to as Control) (Rheinwald and Green, 1977). Sex of the control keratinocytes is unknown because they are derived from the anonymous donors.

**METHOD DETAILS****Cell culture**

Primary keratinocytes were cultured in Keratinocyte Basal Medium supplemented with 100 U/mL Penicillin/Streptomycin, 0.1 mM ethanolamine, 0.1 mM O-phosphoethanolamine, 0.4% (vol/vol) bovine pituitary extract, 0.5 µg/mL hydrocortisone, 5 µg/mL insulin and 10 ng/mL epidermal growth factor. Medium was refreshed every other day. When cells were more than 90% confluent (day 0), differentiation was induced by depletion of growth factors in addition to cell contact inhibition, as described previously (Van Ruisseau et al., 1996). Cells were collected at four differentiation stages, proliferation (day 0), early differentiation (day 2), mid differentiation (day 4), and late differentiation (day 7) for subsequent experiment. No mycoplasma contamination is found during cell culture.

**RNA extraction and quantitative real-time reverse transcription PCR (RT-qPCR)**

Total RNA was isolated using the NucleoSpin RNA kit and quantified with NanoDrop. cDNA synthesis from 1 µg freshly prepared total RNA was carried out using the iScript cDNA synthesis kit. Reverse transcription quantitative PCR (RT-qPCR) primers were designed using Primer3 to obtain exon spanning primers wherever possible. Each primer set has been tested for its linear amplification dynamic range. RT-qPCRs were performed in the CFX96 Real-Time system (Bio-Rad) by using iQ SYBR® Green Supermix according to the manufacturer’s protocol. The human acidic ribosomal protein (*hARP*) or glucuronidase beta (*GusB*) was used as the house-keeping gene for normalization. Differences in the expression of each gene during differentiation (relative expression) were calculated by 2 $\Delta\Delta$ Ct method (Livak and Schmittgen, 2001). Sequences of all RT-qPCR primers were provided in Table S1C.

**Western blotting**

A total of 12.5 µg protein was loaded for each sample. The actin antibody (1:100,000) was used to control equal protein loading. Protein extracts were run on SDS-PAGE and transferred to PVDF membranes using the NuPAGE system (Life Technologies). LumiGLO (Cell Signaling Technology Inc.) was used for chemiluminescent detection by the Bio-Rad Universal Hood Gel Imager (Bio-Rad Laboratories). Antibodies used in this study include LOR (1:2500), RUNX1 (1:50), K18 (1:500). All the original blots were provided in Table S6.

### RNA-seq and analysis pipeline

RNA-seq experiment was performed as described previously (Kouwenhoven et al., 2015a) with the starting material of 500 ng total RNA, to obtain double-strand cDNA (ds-cDNA). After purification with the MinElute Reaction Cleanup Kit, 3 ng ds-cDNA was processed for library construction using KAPA Hyper Prep Kit according to the standard protocol except that a 15-minute USER enzyme incubation step was added before library amplification. The prepared libraries were quantified with the KAPA Library Quantification Kit, and then sequenced in a paired-ended manner using the NextSeq 500 (Illumina) according to standard Illumina protocols.

Sequencing reads were aligned to human genome assembly hg19 (NCBI version 37) using STAR 2.5.0 (Dobin et al., 2013) with default options. A detailed summary of RNA-seq data generated in this study was shown in Table S6A. For data visualization, wigToBigWig from the UCSC genome browser tools was used to generate bigwig files and uploaded to UCSC genome browser. Genes with the mean of DESeq2-normalized counts (“baseMean”) > 10 were considered to be expressed. Differential gene expression (adjusted *P* value < 0.05) and principal-component analysis were performed with the R package DESeq2 using read counts per gene (Love et al., 2014). Hierarchical clustering was performed based on log<sub>10</sub>(FPKM+0.01). Functional annotation of genes was performed with DAVID (Huang da et al., 2009). For Weighted Gene Co-expression Network Analysis (WGCNA (Langfelder and Horvath, 2008)), only high variance genes (adjusted *P* value < 0.01, sum of baseMean > 100, 3162 genes) between control keratinocytes and p63 mutant keratinocytes during differentiation were included. WGCNA clustering within p63 mutant keratinocyte samples was performed using power of 26 and the minimum module size of 15. A total of 16 co-expression modules were identified based on gene co-expression patterns (Table S1J). To visualize the gene network organization, only nodes (genes) with connectivity weight > 0.1 were kept (Table S1K). Cytoscape (Smoot et al., 2011) was used for gene network visualization.

### ChIP-seq and analysis pipeline

Chromatin for ChIP was prepared as previously described (Kouwenhoven et al., 2010). ChIP assays were performed following a standard protocol (Novakovic et al., 2016) with minor modifications. Antibodies against H3K27ac (1.2 μg), H3K4me3 (1 μg), H3K27me3 (1.5 μg), p63 (1 μg, recognizing the C-terminal α tail of p63) and RUNX1 (4 μg) were used in each ChIP assay. Resulted DNA fragments from four independent ChIP assays were purified and subjected to a ChIP-qPCR quality check. Afterward 5ng DNA fragments were pooled and proceeded on with library construction using KAPA Hyper Prep Kit according to the standard protocol. The prepared libraries were then sequenced using the NextSeq 500 (Illumina) according to standard Illumina protocols.

Sequencing reads were aligned to human genome assembly hg19 (NCBI version 37) using BWA (Li and Durbin, 2009). Mapped reads were filtered for quality, and duplicates were removed for further analysis. A detailed summary of ChIP-seq data generated in this study was shown in Table S6B. In addition. The bamCoverage script was used to generate and normalize bigwig files with the RPKM formula. The peak calling was performed with the MACS2 (Zhang et al., 2008) against a reference input sample from the same cell line with standard settings and a *q* value of 0.05. Only peaks with a *P* value < 10e-5 were used for differential analysis with MAnorm (Shao et al., 2012). Association of peaks to genes and associated GO annotation were performed with GREAT (McLean et al., 2010). *P* values were computed with a hypergeometric distribution with FDR correction. *k*-means clustering and heatmap and band plot generation were carried out with a Python package fluff (Georgiou and van Heeringen, 2016). H3K27ac ChIP-seq analyses of control and mutant keratinocytes, including those performed in siRUNX1 experiments, were performed in duplicates. The ‘plot-Correlation’ function from the deepTools package was used and the Pearson correlation coefficient was calculated accordingly (Ramírez et al., 2014).

### ChomHMM analysis

Chromatin states were characterized using ChromHMM v1.11 (Ernst and Kellis, 2012). The peak files from three tracks (H3K27me3, H3K4me3, and H3K27ac) across four stages were used as input. The six-emission state model was determined to be optimal which could sufficiently capture the biological variation in co-occurrence of chromatin marks. The segmentation files of the six emission states per stage were binned into 200 bp intervals. An *M* × *N* matrix was created, where *M* corresponds to the 200 base pair intervals and *N* to the developmental stages (*N* = 4). Each element *x* (*m*, *n*) represents the chromatin state of interval *m* at stage *n*. For each chromatin group, occurrences were counted per stage *N* (Table S2C). The changes between stage *N* and *N*+1 were plotted pairwise using Sankey diagrams (<http://sankeymatic.com/>).

### Motif analysis

Previously described p63scan algorithm was used for p63 motif evaluation (Kouwenhoven et al., 2010). HOMER (<http://homer.ucsd.edu/homer/motif/>) was used for motif scan against corresponding background sequences.

### siRNA nucleofection

Nucleofection was performed as described previously (Mulder et al., 2012) using the Amaxa 96-well shuttle system (Lonza, program FF113). In short, keratinocytes were harvested with Accutase® solution and resuspended in nucleofector buffer SF (Lonza). Each 20 μL transfection reaction contained 200,000 cells mixed with 2 μM validated siRNA (Silencer Select siRNAs, Ambion/Applied Biosystems). In siRUNX1 experiments, siRUNX1-1 oligo was used for the RNA-seq experiment and siRUNX1-2 oligo was used for the western blot experiment. Both siRUNX1 oligoes were used in the RT-qPCR and H3K27ac ChIP-seq experiments. After transfection,

the samples were incubated for 10 minutes at room temperature before resuspension in KBM and seeding at 50,000 cells per well (12 well plate). Medium was refreshed each day for the indicated periods till the end of experiments.

### QUANTIFICATION AND STATISTICAL ANALYSIS

Data are expressed as mean  $\pm$  standard deviation error of the mean unless otherwise specified. Dataset statistics were analyzed using the GraphPad Prism software. Differences under  $p < 0.05$  were considered statistically significant, NS  $P$  value  $> 0.05$ , \*  $P$  value  $< 0.05$ , \*\*  $P$  value  $< 0.01$ , \*\*\*  $P$  value  $< 0.001$ . Gene expression analysis by RT-qPCR was performed in biological duplicates ( $n \geq 2$ ); data are shown as mean  $\pm$  standard deviation, two-way ANOVA. The comparison of gene expression (fold change) was analyzed with the unpaired t test. Hypergeometric test was performed with the online tool GeneProf. The comparison of gene expression after siRNA knockdown was performed with t test. Other statistical methods used in this study were specified in the Figure legends.

### DATA AND SOFTWARE AVAILABILITY

To review dataset of control cells, go to GEO database (accession GSE98483) (<https://www.ncbi.nlm.nih.gov/geo/query/acc.cgi?acc=GSE98483>). To review our complete dataset in Genome Browser, please go to [https://genome.ucsc.edu/cgi-bin/hgTracks?hgS\\_doOtherUser=submit&hgS\\_otherUserName=Jieqiong%20QU&hgS\\_otherUserSessionName=hg19\\_p63\\_RUNX1\\_Jieqiong](https://genome.ucsc.edu/cgi-bin/hgTracks?hgS_doOtherUser=submit&hgS_otherUserName=Jieqiong%20QU&hgS_otherUserSessionName=hg19_p63_RUNX1_Jieqiong)

To review dataset of p63 patient cells, go to dbGaP database (accession phs001737.v1.p1) with controlled access ([https://www.ncbi.nlm.nih.gov/projects/gap/cgi-bin/study.cgi?study\\_id=phs001737.v1.p1](https://www.ncbi.nlm.nih.gov/projects/gap/cgi-bin/study.cgi?study_id=phs001737.v1.p1)).

All data supporting the findings of the study and in-house codes are available on request.